Event generator for Deep Exclusive Meson Production at Jefferson Lab and EIC

Z. Ahmed,[1] R.S. Evans,[1] G.M. Huber,[2,*] S.J.D. Kay,[1] and W.B. Li[3]

[1] *University of Regina, Regina, SK S4S 0A2, Canada*
[2] *University of Regina, Regina, SK S4S 0A2, Canada*
[3] *College of William and Mary, Williamsburg, VA 23187, USA*

(Dated: December 13, 2020)

Background: Measurements of exclusive meson production are a useful tool in the study of hadronic structure...

Purpose: To study the transition between non-perturbative and perturbative Quantum Chromodyanmics...

Method: We have written a physics generator...

Results:

Conclusion:

I. INTRODUCTION

We have written a Deep Exclusive Meson Production (DEMP) event generator, which is modular in form, so that the variety of reactions it simulates can be expanded over time. The motivation for the writing of the event generator is to evaluate the feasibility of hadron structure studies with polarized targets at Jefferson Lab, and with colliding beams at the Electron-Ion Collider.

The process of interest is deep inelastic scattering of an electron and proton. The value of Q^2 is high enough to probe the parton structure via deep inelastic scattering. Deep Exclusive Meson Production is a kind of inelastic scattering in which target nucleon is split in a meson and recoil neutron and either we detect all three outgoing particles or detect two of them with good enough resolution to construct the missing mass and missing momentum. Fig. 1 shows the deep exclusive meson production. DEMP has larger contributions from higher twist at amplitude level, but these contributions cancel out in some asymmetries.

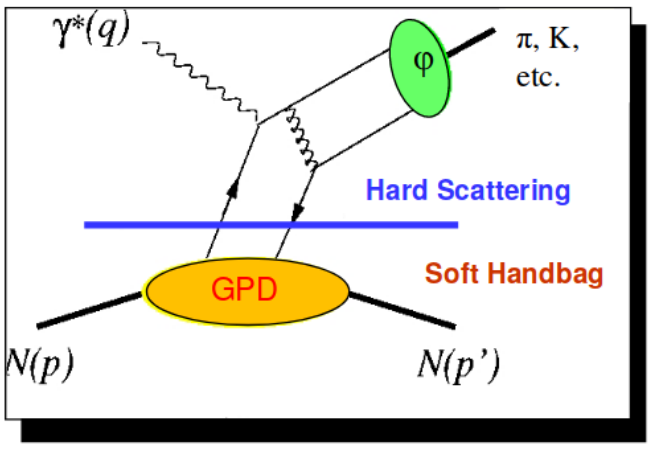

FIG. 1. DEMP handbag diagram for the factorization regime at large Q^2

The physics event generator is written in a modular form, so the different physics processes that can be generated can be easily expanded over time. At present, three physics processes are available:

1. Exclusive $^3He(e,e'\pi^-)p(pp)_{sp}$ events from the polarized neutron in a polarized ^{3}He target for Jefferson Lab. The generator allows the neutron Fermi momentum and other nuclear effects to be easily turned on and off for various studies.

2. Exclusive $p(e,e'\pi^+n)$ events in colliding beam mode for the EIC, where the π^+ is emitted at small $-t$, at forward angles in the center of mass frame.

3. u-channel exclusive $p(e,e'p\pi^0)$ events in colliding beam mode for the EIC. In the center of mass frame, the π^0 travels in the backward direction, with the forward going proton taking most of the momentum.

This paper is divided into sections as follows. In Sec. II we will briefly describe the scientific motivation for our studies, so the structure and kinematic ranges of applicability of the generator can be better understood. In Sec. III, we summarize the coding structure of the generator, and the cross section parameterization of the different physics processes. In Sec. IV we present some results obtained with the generator, to display some of the ways in which it can be used. Sec. V presents a summary of our work to date, and an outlook of some extensions to the generator that are being considered.

II. SCIENTIFIC MOTIVATION FOR OUR STUDIES

A. Motivation for Jefferson Lab $\vec{n}(e,e'\pi^-)p$ studies

The over-arching goal is to understand the structure of hadrons in terms of partons. The process of interest is deep inelastic scattering (DIS) and quantum chromodynamics is the underlying theory of interaction. The purpose of our studies is to obtain an improved picture of hadrons with the help of Generalized Parton Distributions.

At leading twist, there are four GPDs $H(x,\xi,t)$, $E(x,\xi,t)$, $\tilde{H}(x,\xi,t)$ and $\tilde{E}(x,\xi,t)$ associated with each quark flavor. H and $\tilde{H}$ GPDs conserve helicity and the E and $\tilde{E}$ GPDs are associated with an helicity flip of the nucleon. Each GPD depends upon three variables which are average longitudinal momentum fraction of struck quark x and in high Q^2 regime $x = x_B$, skewness ξ and four momentum transfer Q^2. GPDs also describe the correlation between partons in a nucleon.

* Email: huberg@uregina.ca

By Fourier transform we can access simultaneously the longitudinal momentum fraction of quarks and their position in the transverse plane [1].

First moments of GPD are related to elastic form factors of the nucleon. GPDs integral over x gives [2]:

$$\int_{-1}^{1} dx \quad H^q(x,\xi,t) = F_1^q(t) \tag{1}$$

$$\int_{-1}^{1} dx \quad E^q(x,\xi,t) = F_2^q(t) \tag{2}$$

$$\int_{-1}^{1} dx \quad \tilde{H}^q(x,\xi,t) = g_A^q(t) \tag{3}$$

$$\int_{-1}^{1} dx \quad \tilde{E}^q(x,\xi,t) = h_A^q(t) \tag{4}$$

where F_1, F_2, g_A and h_A are Dirac, Pauli, pseudoscaler and vector form factors. The relation between one quark flavor form factor and proton form factor is given by: [3]

$$F^{u/p} = 2F_1^p + F^n + F_1^s \tag{5}$$

$$F^{d/p} = 2F_1^n + F^p + F_1^s \tag{6}$$

$$g_A^u = \frac{1}{2}g_A + \frac{1}{2}h_A^0 \tag{7}$$

$$g_A^d = -\frac{1}{2}g_A + \frac{1}{2}g_A \tag{8}$$

GPDs give the information about the nucleon independent of the reaction. We can measure GPDs via DEMP. Virtual photon in DEMP has longitudinal component of polarization. The transverse component is suppressed by $1/Q^2$ compared to longitudinal component. I am quoting [3]:
"Because the quark helicity is conserved in the hard scattering process, the meson acts as a helicity filter. In particular, the leading order perturbative QCD predicts [Col97] that the longitudinally polarized vector meson channels ($\rho_L^{0,\pm}, \omega_L, \phi_L$) are sensitive only to the unpolarized GPDs (H and E) whereas the pseudo scalar channels ($\pi^{0,\pm}, \eta, ...$) are sensitive only to the polarized GPDs ($\tilde{H}$ and $\tilde{E}$). In comparison to meson electroproduction reactions, we rec all that DVCS depends at the same time on both the unpolarized (H and E) and polarized ($\tilde{H}$ and $\tilde{E}$) GPDs. This property makes the hard meson electroproduction reactions complementary to the DVCS process, as it provides an additional tool to disentangle the different GPDs".

GPD $\tilde{E}$ not related to an already known parton distribution. Experimental information on $\tilde{E}$ can provide new nucleon structure info unlikely to be available from any other source. The most sensitive observable to probe $\tilde{E}$ is the transverse single spin asymmetry in exclusive π production:

$$A_L^{\perp} = \frac{\int_0^{\pi} d\beta \frac{d\sigma_L^{\pi}}{d\beta} - \int_{\pi}^{2\pi} d\beta \frac{d\sigma_L^{\pi}}{d\beta}}{\int_0^{2\pi} d\beta \frac{d\sigma_L^{\pi}}{d\beta}} \tag{9}$$

where $d\sigma_{\pi}^L$ is exclusive π cross section for longitudinal virtual photons and β is angle between transversely polarized target vector and the reaction plane.

Frankfurt et al. have shown $A_L^{\perp}$ vanishes if $\tilde{E}$ is zero [4]. If $\tilde{E} \neq 0$ the asymmetry will produce a $sin(\beta)$ dependence.

B. Motivation for EIC π^+ studies

The Electron-ion collider is the next generation collider to study the structure of nucleon. An Electron ion collider (EIC) is designated as the high priority new construction project in the 2015 Nuclear Physics Long Range Plan by NSAC, United States. According to EIC white paper [5] it will answer these three questions:

- How are the sea quarks and gluons, and their spins, distributed in space and momentum inside the nucleon?
- Where does the saturation of gluon densities set in?
- How does the nuclear environment affect the distribution of quarks and gluons and their interactions in nuclei?

quoting [5]:

Answers to these questions are essential for understanding the nature of visible matter. An EIC is the ultimate machine to provide answers to these questions for the following reasons:

- A collider is needed to provide kinematic reach well into the gluon-dominated regime.
- Electron beams are needed to bring to bear the unmatched precision of the electromagnetic interaction as a probe.
- Polarized nucleon beams are needed to determine the correlations of sea quark and gluon distributions with the nucleon spin.
- Heavy ion beams are needed to provide precocious access to the regime of saturated gluon densities and offer a precise dial in the study of propagation-length for color charges in nuclear matter.

The Pion is the most simple hadronic system available to study the structure of hadrons and provides various tests for QCD. One of the experimentally feasible approaches is the Electroproduction of Pion from a nucleon. The polarized quark distribution in the proton can be examined by hard electroproduction of pseudoscalar mesons like *pion* and *kaon*. The Pion form factor $\mathbf{F}_{\pi}(Q^2)$ is measured in Hall C via Electroproduction of Pions up to $Q^2 = 2.45$ GeV^2 with high precision [6]. Jlab experiment E12-06-101 is approved with A rating to measure the Pion form factor at high Q^2 value. This experiment will provide the information about $\mathbf{F}_{\pi}(Q^2)$ in the "soft" and "hard" regions of QCD. Measurement of pion form factor at EIC is continuation of this study of the pion form factor at higher Q^2 kinematics.

The elastic electromagnetic form factors of the charged pion and kaon, $F_{\pi}(Q^2)$ and $F_K(Q^2)$, are a rich source of insights into basic features of hadron structure, such as the

roles played by confinement and Dynamical Chiral Symmetry Breaking (DCSB) in fixing the hadron's size, determining its mass, and defining the transition from the strong- to perturbative-QCD domains. Studies during the last decade, based on JLab 6-GeV measurements, have generated confidence in the reliability of π^+ electroproduction as a tool for pion form factor extractions. Forthcoming measurements at the 12-GeV JLab will deliver pion form factor data that are anticipated to bridge the region where QCD transitions from the strong (color confinement, long-distance) to perturbative (asymptotic freedom, short-distance) domains.

At the EIC, pion form factor measurements can be extended to still larger Q^2, by measuring ratios of positively- and negatively-charged pions in quasi-elastic electron-pion (off-shell) scattering via the $p(e,e'\pi^+)n$ and $n(e,e'\pi^-)p$ reactions, accessed with proton and deuterium beams. The measurements would be over a range of small $-t=-(p_p-p_n)^2$, and gauged with theoretical and phenomenological expectations, to again verify the reliability of the pion form factor extraction at EIC kinematics.

The experimental determination of the π^+ electric form factor (F_π) is challenging. The best way to determine F_π would be electron-pion elastic scattering. However, the lifetime of the π^+ is only 26.0 ns. Since π^+ targets are not possible, and π^+ beams with the required properties are not yet available, one must employ high-energy exclusive electroproduction, $p(e,e'\pi^+)n$. This is best described as quasi-elastic (t-channel) scattering of the electron from the virtual π^+ cloud of the proton, where t is the Mandelstam momentum transfer $t=(p_p-p_n)^2$ to the target nucleon. Scattering from the π^+ cloud dominates the longitudinal photon cross section ($d\sigma_L/dt$), when $|t|\ll m_p^2$ [7]. To reduce background contributions, normally one separates the components of the cross section due to longitudinal (L) and transverse (T) virtual photons (and the LT, TT interference contributions), via a Rosenbluth separation. The value of $F_\pi(Q^2)$ is determined by comparing the measured $d\sigma_L/dt$ values at small $-t$ to the best available electroproduction model. The obtained F_π values are in principle dependent upon the model used, but one anticipates this dependence to be reduced at sufficiently small $-t$. Our JLab 6 GeV experiments were instrumental in establishing the reliability of this technique up to $Q^2=2.45$ GeV^2 [6], and extensive further tests are planned as part of JLab E12-19-006 [8].

The reliability of the electroproduction method to determine the K^+ form factor is not yet established. JLab E12-09-011 has acquired data for the $p(e,e'K^+)\Lambda$, $p(e,e'K^+)\Sigma^0$ reactions at hadronic invariant mass $W=\sqrt{(p_K+p_{\Lambda,\Sigma})^2}>2.5$ GeV, to search for evidence of scattering from the proton's "kaon cloud". The data are still being analyzed, with L/T-separated cross sections expected in the next ∼2 years. If they confirm that the scattering from the virtual K^+ in the nucleon dominates at low four-momentum transfer to the target $|t|\ll m_p^2$, the experiment will yield the world's first quality data for F_K above $Q^2>0.2$ GeV^2. This would then open up the possibility of using the same exclusive reactions to determine the kaon form factor over a wide range of Q^2 at the EIC.

C. Motivation for backward region (π^0 DEMP)

The collinear QCD factorization property, which ensures the validity of the GPD-based description of near-forward ($t\sim t_{min}$) DVCS,TCS and DVMP, may be extended to the complementary near-backward kinematics ($u\sim u_{min}$) regime provided that the GPD is replaced by a baryon-to-meson Transition Distribution Amplitude (TDA), as demonstrated in Fig. 2 left plot. TDAs are opening a new window on the study of the 3-dimensional structure of nucleons and recent experimental analysis of backward exclusive electroproduction of π^+ (CLAS 6) [9] and ω (JLab Hall C) [9, 10] indicate that this concept may be applicable at moderate values of Q^2.

The recently approved JLab 12 GeV experiment E12-20-007 aims to further study and validate TDA by probing exclusive electroproduction interaction: ^{1}H$(e,e'p)\pi^0$, in the kinematics range: $2<Q^2<6.25$ GeV^2 at fixed $W=3.1$ GeV ($s=10$ GeV^2) and. The proposed measurement will utilize the 12 GeV e beam on an unpolarized liquid hydrogen target (LH_2), in combination with the high precision spectrometers available at Hall C of Jefferson Lab. The key observable involves detecting scattered electrons and fast recoiled protons, and resolving π^0 events using the missing mass reconstruction technique. The separated cross section: σ_T , σ_L and σ_T/σ_L ratio at 2-5 GeV^2, directly challenges the two remarks postulated by the TDA model: $\sigma_T=1/Q^8$ and $\sigma_T\gg\sigma_L$ in the u-channel kinematics. This will be an important step forward in validating the existence of a backward factorization scheme of the nucleon structure function and establishing its applicable kinematics range.

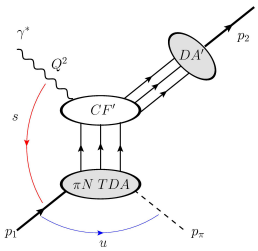

FIG. 2. The π^0 electroproduction through $\gamma^*p\to p\pi^0$, under the (backward-angle) TDA colinear factorization regime (large Q^2, large s, fixed x_B, $u\sim u_{\min}$). The πN TDA (bottom grey oval) is the transition distribution amplitude that transform a nucleon to a vector meson. The fast froward-going nucleon is described by the DA (top-right oval).

Fig. 2 right plot, illustrates the perspective of Q^2 ($10<Q^2<10$ GeV^2) evolution combining backward ($u\sim u_{min}$) exclusive π^0 production data from JLAB, PANDA and EIC, at fixed $W=10$ GeV. Preliminary study has confirmed the feasibility of studying the interaction: $e+p\to e'+p'+\pi^0$, in the range: $6.25<Q^2<10.0$ GeV^2. The EIC offers unique opportunity to provide definitive test to TDA predictions beyond JLab 12 GeV kinematics. Furthermore, the EIC result is anticipated to play a significant role in the extraction of TDAs.

III. DEMP EVENT GENERATOR

In this section, we will describe the structure of the generator, as well as the parametrization, kinematics ranges and scattering cross section for each of the DEMP processes.

In EIC, we have proton beam up to 100 GeV and electron beam up to 10 GeV. Both beams are crossing at an angle of 25 mrad. All the three outgoing particles, electron, pion and neutron are detected. Proton beam is making an angle of 25 mrad with z axis and electron beam is going in $-\hat{z}$ direction.

A. Structure

Fig. 3 demonstrates the flow of data in the event generator, starting from random number generators, leading to the output file. The rounded boxes in this chart each indicate the main named variables whose values are pointers to instances of the indicated class. For example, "VertTargNeut" is a pointer to an object of class "Particle". These variables, the classes, and their place in the structure of the event generator are discussed in the following subsections.

Instances of the particle class contain all of the pieces of information about a single particle, in a single frame of reference, that are relevant to the event generator. This includes the four-momentum, rest mass, charge, etc. The particle inherits from ROOT's TLorentzVector class, which allows for the creation and manipulation of general four-vectors. The TLorentzVector class includes methods to calculate components, angles, and magnitudes of a four-momentum, as well as perform Lorentz boosts and rotations. It also defines algebraic operators for four-vectors. Implementation of this class significantly simplifies calculations within the event generator, and eliminates a large number of messy algorithms that were present in the original event generator.

Instances of the DEMPEvent class represent the event viewed from a single reference frame. The class stores seven particle objects: The incident electron, target neutron, virtual photon, scattered electron, produced pion, and recoiled proton. The class has methods to calculate Mandelstam variables s, t, u, and functions to perform coordinate transformations on the event. There are five DEMPEvent objects initialized in the event generator, as seen in Fig. 3. VertEvent contains the particles as viewed at the vertex of the interaction, in the laboratory rest frame. Once the kinematics calculations have been completed (see Section III B), this object is no longer modified. All other DEMPEvent objects are calculated from this object by copying and then transforming them. CofMEvent is the event viewed at the vertex in the center of momentum reference frame. RestEvent is the event viewed at the vertex in the rest frame of the target neutron. TConEvent is the event viewed at the vertex in the coordinate system defined by the Trento Conventions [11].

B. Kinematics

Calculation of of particle kinematics begins with random generation of the energy and momentum of the target neutron, if Fermi momentum is enabled. If Fermi momentum is not enabled it is set to zero momentum, with energy equal to the neutron rest mass. Next, the energy of the scattered electron is selected from a uniform random distribution in a configurable range (typically 0.1 to 0.9 times the energy of the incident beam). The direction of the scattered electron is selected using sphere point picking [12]. The azimuthal angle (ϕ) may be selected from a uniform distribution form 0 to 2π, but selecting the polar angle (θ) uniformly results in bunching near $\theta = 0$. The distrubtion function for the polar angle is instead $\frac{1}{2}\sin^2(\theta)$. The direction for the produced pion is then selected, again using sphere point picking. The energy of the pion is left to be solved for.

These variables provide all information necessary to uniquely solve for the rest of the kinematic variables. Applying conservation of energy and momentum yields the following equation:

$$\gamma^0 + n^0 - \sqrt{m_\pi^2 + |\vec{\pi}|^2} - \sqrt{m_p^2 + |\vec{\gamma} + \vec{n} - \vec{\pi}|^2} = 0 \quad (10)$$

where γ^0 and n^0 represent the 0th component of the four-momentum (energy) of the virtual photon and neutron respectively. The vectors represent the three-momentum of their respective particles. The only unknown in this equation is the momentum vector of the pion. Since the direction of the pion has already been specified, Equation 10 may be futher reduced to a single-valued unknown: the momentum magnitude of the pion.

The left hand side of the equation is defined in the event generator as a function of $|\vec{\pi}|$ in a ROOT TF1 (1-Dim function) object. The TF1 object incorporates a root finding algorithm, using Brent's method [13], which is used to find values for $|\vec{\pi}|$ which solve Equation 10. If more than one solution is found, one is picked at random.

The energy and momentum of the proton can then be calculated by a straightforward application of conservation of four-momentum. The following checks are then made to verify that solution is within acceptable limits: The rest mass of the proton is calculated from the solution and compared against the known value, the value of Mandelstam variable W for the initial state is compared to the final state, and total energy and momentum for the initial state is compared to final state. If any value deviates by more than 1 MeV(/c), or a solution is not found, the event is discarded. In testing over several million events, all events with solutions passed these checks, however approximately a third of events did not have a solution and were discarded.

C. Event Weighting

Three outgoing particles (e', π and n)are generated in collider frame. First we generate a scattered electron with random direction and momentum. Range of θ , ϕ and magnitude of momentum of scattered electron are defined by phase space. Then we randomly generate θ and ϕ of pion as defined by phase space. Then we use the method given in SIMC [14] to find the momentum of pion analytically. Then we generate the direction and momentum of neutron by applying the law of conservation of energy and momentum. Finally the cross section is given in collider frame.

When event generator asks you to input the number of events it is the number of events it will try to generate. Actual number of generated events will be different (smaller)

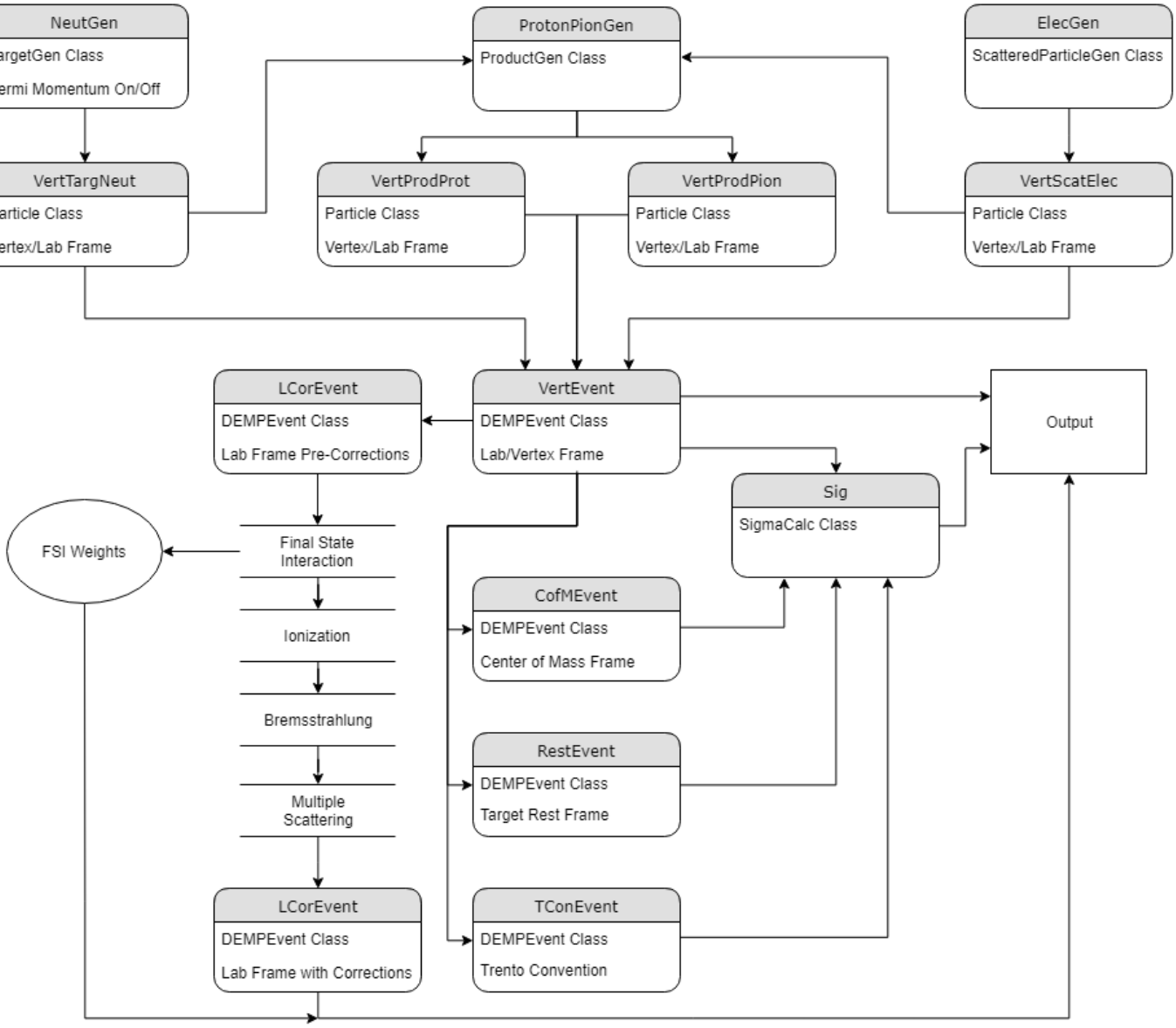

FIG. 3. Flowchart describing the flow of data through the program, and the structure of the event generator. The rounded boxes signify the most important named variables that appear in the main file of the program. Their values that are pointers to an instance of the given class. Arrows indicate how data is moved between these objects. The four open boxes indicate static functions. The "FSI Weights" node represents a simple collection of doubles. The "Output" box represents destination for data to be saved into the output ROOT tree.

then the events tried. Generated evetns are normalize to number of events tried. Event weight is calculated for each event in the following way:

$$weight = \text{cross section} \times \text{Phase Space} \times Conversion \times Luminosity/\text{Total events tried} \quad (11)$$

Conversion factor converts microbrans to cm^2. Unit of event weight is Hz. Output of event generator are a root file and a lund file.

D. Exclusive $p(e, e'\pi^+)n$ Physics Model

This generator is based upon the Regge model of Tae Keun Choi, Kook Jin Kong and Byung Geel Yu [15]. This model provides an excellent description of the existing JLab data up to $-t$=4.3 GeV^2 [16] and is well-behaved over a wide kinematic range. We have performed simulations demonstrating the feasibility of pion electric form factor measurements at the EIC using this event generator. Depending on the success of the K^+ form factor experiment (JLab E12-09-011), we can modify this generator for the exclusive $K^+\Lambda$ channel, and investigate the feasibility of these measurements at EIC in 2021–23.

Simulation study of this DEMP process requires differential cross section associated with each event. For our event generator the ranges of different variables over which we generate the events are given in the table I.

The following three Lorentz invariants are used to define the kinematics:

Kinematic ranges for the reaction	
$\theta_{e'}$	from 175 to 60 degrees
$E_{e'}$	from 2.5 GeV (50% of E_e) to 12.5 GeV (250% of E_e)
$\phi_{e'}$	0 to 360 degrees
θ_π	from 0 to 50 degrees
ϕ_π	0 to 360 degrees
Q^2	from 5 GeV^2 to 35 GeV^2
$-t$	up to 0.5 GeV^2(FF), up to 1.3 GeV^2(TSSA)[17]
W	rom 2 to 10 GeV
x_B	up to 0.5
ξ	up to 0.4
Luminosity	$3.7 \times 10^{32}/(cm.s)$

TABLE I. Kinematics

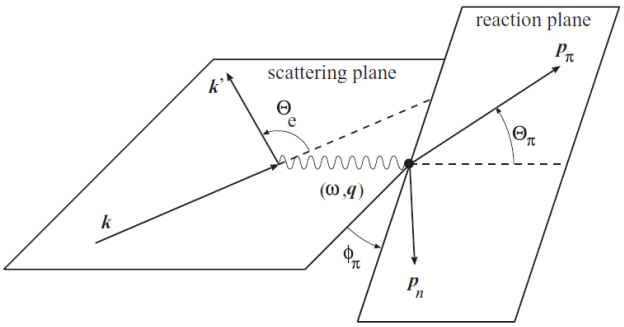

FIG. 4. The scattering and reaction planes in exclusive π^+ electroproduction, and definitions of the relevant Lorentz invariant quantities.

$$-Q^2 = (k - k')^2 \tag{12}$$

$$W^2 = (p_\gamma + p_p)^2 = (p_\pi + p_n)^2 \tag{13}$$

$$t = (p_\gamma - p_\pi)^2 = (p_p - p_n)^2 \tag{14}$$

The scattering cross section for DEMP in one-photon exchange is given by equation 15 with incoming and outgoing electrons described as plane waves:

$$\frac{d^5\sigma}{dE' d\Omega_{e'} d\Omega_\pi} = \Gamma_V \frac{d^2\sigma}{d\Omega_\pi}. \tag{15}$$

The five fold cross section of equation 15 is then transformed to lab(collider) frame with an additional Jacobian. The virtual photon flux factor Γ_V in equation 15 is the virtual flux factor defined in the Hand convention:

$$\Gamma_v = \frac{\alpha}{2\pi^2} \frac{E'}{E} \frac{K}{Q^2} \frac{1}{1-\epsilon}, \tag{16}$$

where α is the fine structure constant, K is the energy of real photon equal to the energy of photon energy required to create a system with invariant mass equal to W and ϵ is the polarization of the virtual photon.

$$K = (W^2 - M_p^2)/(2M_p) \tag{17}$$

The two-fold differential cross section in lab frame can be expressed in terms of the invariant cross section in center of mass frame of the photon and proton:

$$\frac{d^2\sigma}{d\Omega_\pi} = J \frac{d^2\sigma}{dt d\phi}, \tag{18}$$

$$2\pi \frac{d^2\sigma}{dt d\phi} = \epsilon \frac{d\sigma_{\rm L}}{dt} + \frac{d\sigma_{\rm T}}{dt} + \sqrt{2\epsilon(\epsilon+1)} \frac{d\sigma_{\rm LT}}{dt} \cos\phi + \epsilon \frac{d\sigma_{\rm TT}}{dt} \cos 2\phi \tag{19}$$

where subscript L and T are for longitudinal and transverse polarizations of virtual photon, ϕ is defined in Fig. 4, and J is given below. The longitudinal photon polarization parameter, ϵ, is given by:

$$\epsilon = \left(1 + \frac{2|\mathbf{q}|^2}{Q^2} \tan^2 \frac{\theta_e}{2}\right)^{-1} \tag{20}$$

In the study of DEMP at EIC, we ignore the cross terms σ_{LT} and σ_{TT}, which arise from longitudinal transverse and transverse transverse interference states of the virtual photon, as they are small, and even more highly uncertain than σ_L and σ_T.

Finally, we transform the five fold cross section to the collider frame with the help of following Jacobians.

$$J = A \times J_{rf}^{col} \tag{21}$$

$$J_{rf}^{col} = \frac{|\vec{p}_\pi|^2 \times W}{|\vec{p}_\pi^{cm}|(M_p + E_\gamma)|\vec{p}_\pi| - E_\pi |\vec{p}_\gamma| cos(\theta_\pi)|} \tag{22}$$

$$A = J_{cm} \frac{|\vec{p}_\pi^{cm}|}{\pi} \tag{23}$$

$$J_{cm} = \frac{\vec{p}_\gamma^{rf} - \beta_{cm}^{rf} E_\gamma^{rf}}{\gamma_{cm}^{rf}(1 - (\beta_{cm}^{rf})^2)} \tag{24}$$

1. *Weiss model, VR Model and CKY model*

Christian Weiss has provided us a model for DEMP for high Q^2[18]. Weiss model is valid for $W^2 >> Q^2$, $W >> 2$ GeV and small x. The Weiss model is base on a Reggized Born term for high energy photoproduction, including a vector dominance like Q^2 of electroproduction at Q^2 ¡¡ 1 GeV^2, and extrapolation to high Q^2 assuming pQCD scaling behavior. The VR model [19] by Tom Vrancx and Jan Ryckebusch introduces a strong hadronic form factor in the Reggeized background amplitudes. "Hadronic models corrected for resonance/parton duality describe the separated pion electroproduction cross sections above the resonance region reasonably well at low -t". VR model is works very well for $-t$ up to 0.9 GeV^2. The CKY [15] model is proposed by Tae Keun Choi, Kook Jin Kong and Byung Geel Yu. It is also a Regge based model. The CKY model take account of the importance of the roles of pion and proton form factors in DEMP. There is an excellent

agreement between VR model and CKY model. CKY model works well for -t up to 1.5 GeV^2

In order to make the event generator more efficient and save CPU time, we applied some hard cuts. We ignored the events with $Q^2 < 5$ GeV^2, $W < 3$ GeV, $W > 10.6$ GeV and if its FF(Form Factor) generator then $-t > 0.6$ GeV^2 or if TSSA (Transverse Single Spin Asymmetry) generator then $-t > 1.3GeV^2$. Please note that TSSA part of generator is incomplete. I will explain later what is needed to be done.

For parametrization we have range of Q^2 from 3 to 35 GeV^2, range of W is from 2 to 10.2 GeV and range of -t is up to 1.3 GeV^2. We have 22 bins of W. Each W bin is 0.2 GeV wide. For each W bin we have 33 Q^2 bins. Each Q^2 bin 1 GeV^2 wide. Finally in each unique bin of Q^2 and W we plotted σ_L (Fig. 5) and σ_T (Fig. 6) against $-t$.

2. Comparison of three models

For EIC kinematics for FF and TSSA we did a detailed comparison of Weiss model, VR model and CKY model for σ_L and σ_T. A typical graph of each sigma is shown in Figs. 5, 6. For the kinematics of interest the Weiss model is more than the VR and CKY models by 2 or 3 times of magnitude. The agreement in σ_L for low $-t$ is much better but still Weiss model is ate least 2 times greater than VR and CKY models. Weiss model is valid for events which has $W^2 \gg Q^2$ which is the case most of the time in EIC kinematics but not true all the time. For σ_T Weiss model is more than VR and CKY models by 2 to 10 times of magnitude. We can see from the figure that VR model and CKY model are in good agreement with each other.

3. Parametrization of σ_L

We parameterized the CKY model for the calculation of the π^+ production cross section. Math library of ROOT [13] is used to parameterized σ_L. In our parametrization range of W is from 2 GeV to 10 GeV. This range is divided in 41 bins of same with of 0.2 GeV. For reach W bin range of Q^2 goes from 5 to 35 GeV^2 and width of each Q^2 bin is 1 GeV^2. For each unique bin of W and Q^2 we parameterized σ_L and σ_T against the values of $-t$ from 0 to 1.3 GeV^2.

When and event is generated with a value of Q^2 generator looks for rounded up integer value and get the cross section value. Same is done for W. This is done to keep a conservative approch.

Cross terms σ_{LT} and σ_{TT} are small so they are ignored.

σ_L is parameterized with a Landau function $\mathcal{L}_{Landau}$ and two exponential functions as described below:

$$\sigma_L(Q^2_{bin}, -t, W_{bin}) = \begin{cases} \mathcal{L}_{Landau}, & 0 \geq -t < 0.15 \\ exp(c_1 + c_2|-t|), & 0.15 \geq -t < 0.5 \\ exp(c_3 + c_4|-t|), & 0.5 \geq -t < 1.3 \end{cases} \quad (25)$$

For analytic expression of $\mathcal{L}_{Landau}$ please see ROOT documentation.

4. Parametrization of σ_T

σ_T is parameterized with a second order polynomial function of $-t$ up to 0.2 GeV^2 and then with an exponential function of -t for $0.2 < -t < 1.3$ for each bin of Q^2 and W.

$$\sigma_T(Q^2_{bin}, -t, W_{bin}) = \begin{cases} c_0 + c_1|-t| + c_2|-t|^2, & 0 \geq -t < 0.2 \\ exp(c_3 + c_4|-t|), & 0.2 \geq -t < 1.3 \end{cases} \quad (26)$$

E. Exclusive $^3He(e, e'\pi^-)p(pp)_{sp}$ Physics Model

1. Parameterization of σ_{UU}

The unpolarized cross section, $d\sigma_{UU}$, shorthanded as σ_{UU}, and its components are parameterized from the phenomenological Vrancx-Ryckebusch (VR) model [19]. Model data are generated in the kinematic region of Q^2 from 4.0 to 7.5 GeV^2, $-t$ from $-t_{min}$ to -1.0 GeV^2, and at $W = 3.0$ GeV [19] [20] [21]. The W dependence is then taken as $(W^2 - M_p^2)^{-2}$, where M_p is the proton mass [22].

These data were parameterized to fit the following functions:

$$\sigma_L = \exp\left(P_1(Q^2) + |t| * P_1'(Q^2)\right) + \exp\left(P_2(Q^2) + |t| * P_2'(Q^2)\right), \quad (27)$$

$$\sigma_T = \frac{\exp\left(P_1(Q^2) + |t| * P_1'(Q^2)\right)}{P_1(|t|)}, \quad (28)$$

$$\sigma_{LT} = P_5(t(Q^2)), \quad (29)$$

$$\sigma_{TT} = P_5(t(Q^2)). \quad (30)$$

The results of this parameterization were hard-coded into functions for use in the original event generator. These functions are incorporated into the new event generator and accessed by the SigmaCalc class.

2. Parameterization of Azimuthal Modulations

S. V. Goloskokov and P. Kroll have provided model data for the $k = 1 - 5$ asymmetry amplitudes [23]. These data are at discrete values of Q^2 from 4.107 to 7.167 GeV^2, W from 2.362 to 3.191 GeV, and $t' = t - t_{min}$ from 0 to 0.5 GeV^2. t is the momentum transfer $t = (q - p_{\pi^-})^2$ (where q and p_{π^-} are the four momenta of the virtual photon and produced pion, respectively) and t_{min} is the minimum value of t for a constant Q^2 and W. The raw GK model data are shown in Fig. 9. The sixth asymmetry amplitude is expected to be much smaller and is taken to be zero.

The fit functions were initially chosen only to closely match the shape of the model data, and were not based on any physical principle. They are as follows:

$$A_{UT}^{\sin(\mu\phi + \lambda\phi_s)_k} = \begin{cases} ae^{bt'} - (a + c)e^{dt'} + c, & k = 1 \\ ae^{bt'} + c, & k = 2, 3, 4, 5 \end{cases} \quad (31)$$

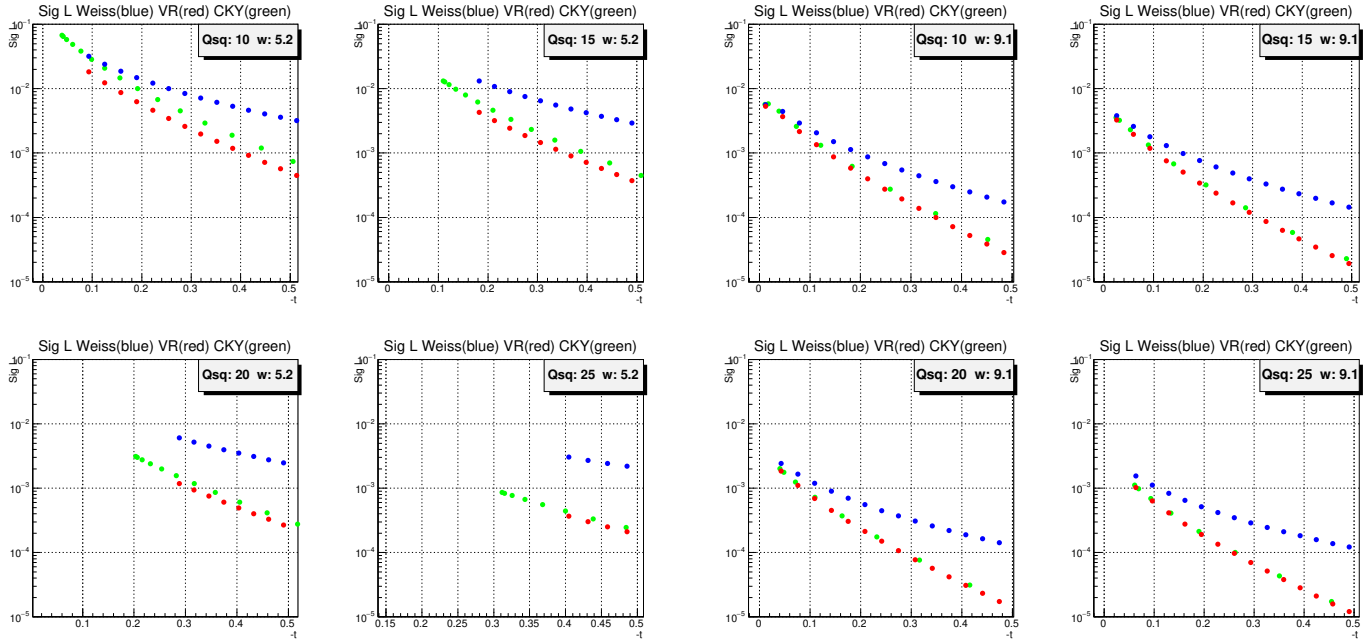

(a) (b)

FIG. 5. Comparison of Weiss model, VR model CKY model for σ_L at W =5.2 (left) and 9.1 (right).

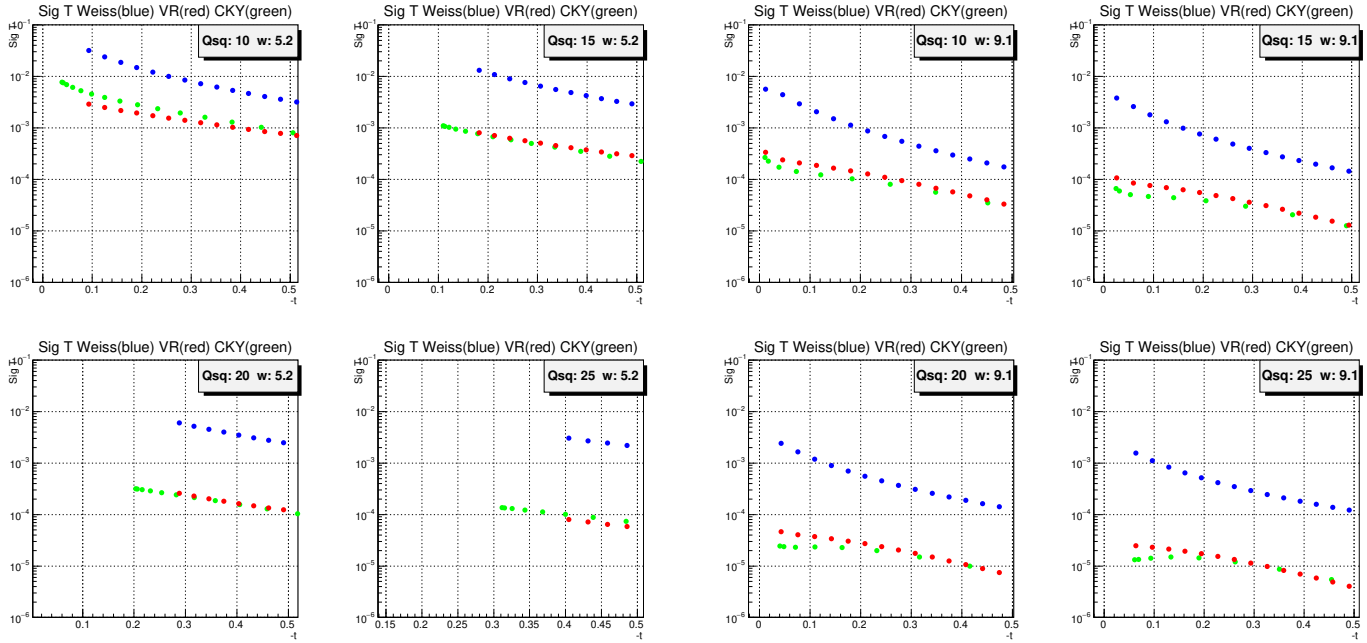

(a) (b)

FIG. 6. Comparison of Weiss model, VR model CKY model for σ_T at W =5.2 (left) and 9.1 (right).

where a, b, c, and d are fit parameters. These fits are done independently for each Q^2, W pair. The parameterized functions are displayed alongside the model data in Fig. 9. The $k = 1$ fit function originally had an additional, independent parameter in place of $(a+c)$, but the fit did not converge reliably. As such, it was constrained to pass through the origin, justified by the requirement that all asymmetries dependent on ϕ must vanish at $t = t_{min}$, as ϕ is undefined in parallel kinematics. This also applies to all but the $k = 3$ asymmetry, however, the fits were satisfactory, and the additional constraint was not deemed necessary.

The main physics goal of the DEMP experiment is to measure the $k = 1$ asymmetry amplitude, $A_{UT}^{\sin(\phi-\phi_s)}$. In addition, the $k = 3$ asymmetry amplitude, $A_{UT}^{\sin(\phi_s)}$, may also be accessible through this experiment, and gives information on higher order GPDs.

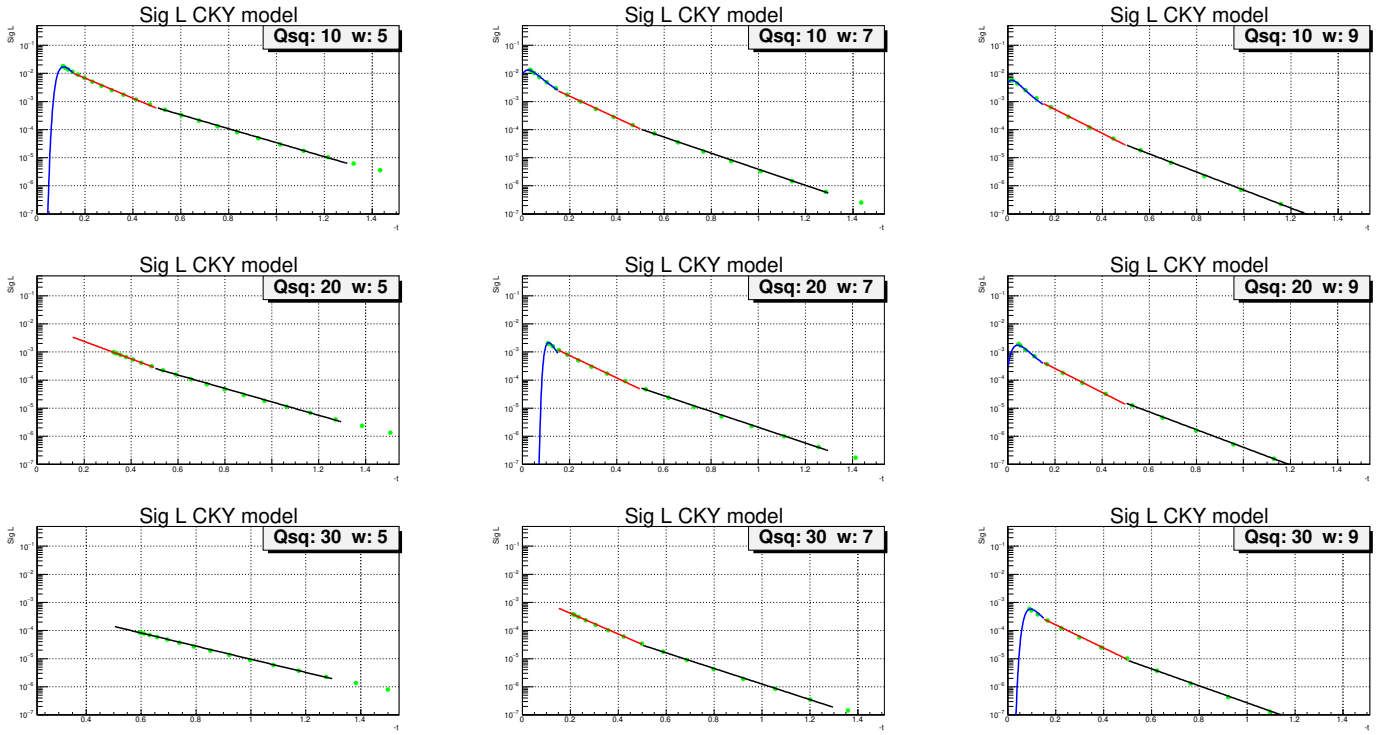

(a) (b) (c)

FIG. 7. Parametrization of CKY σ_L. CKY model values are green circles. Landau function shown in blue. Red and black are two exponentials.

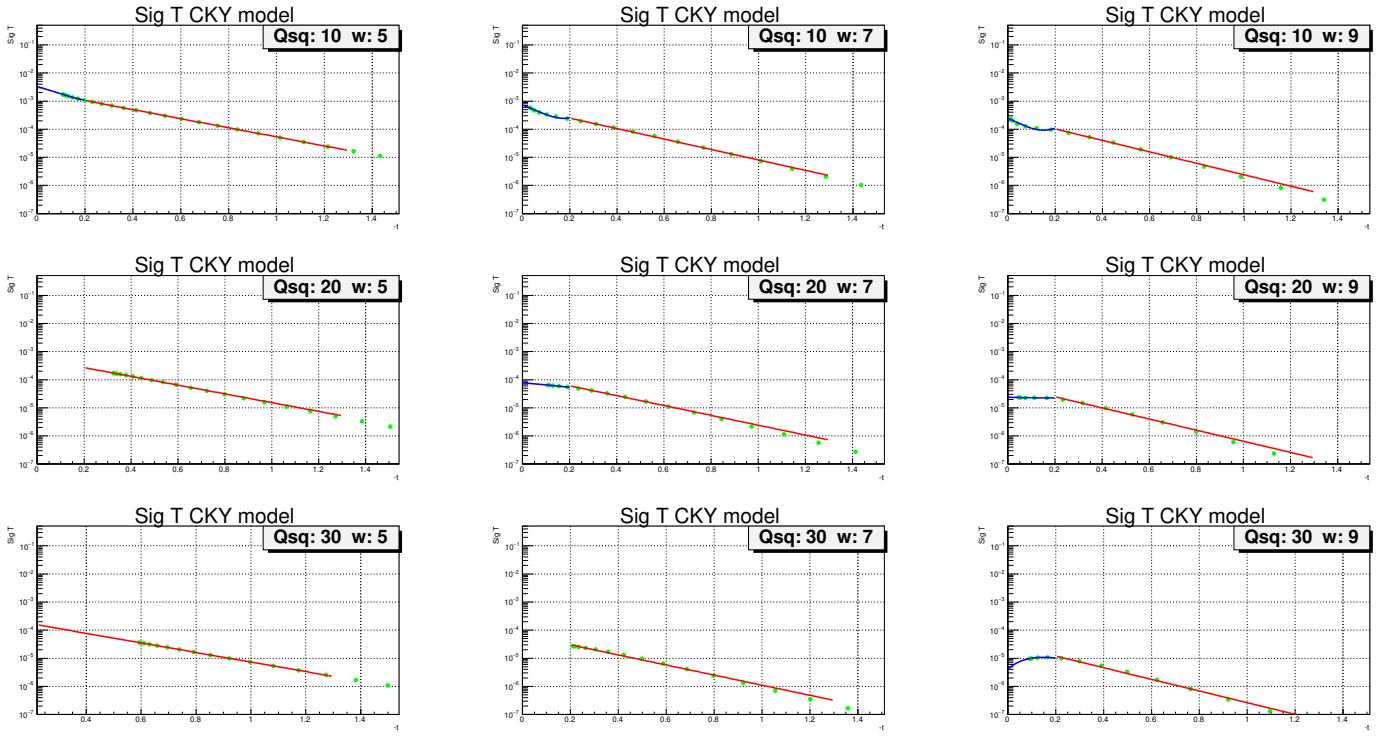

(a) (b) (c)

FIG. 8. Parametrization of CKY σ_T. CKY model values are green circles. Second order polynomial is shown in blue and Red is exponential function.

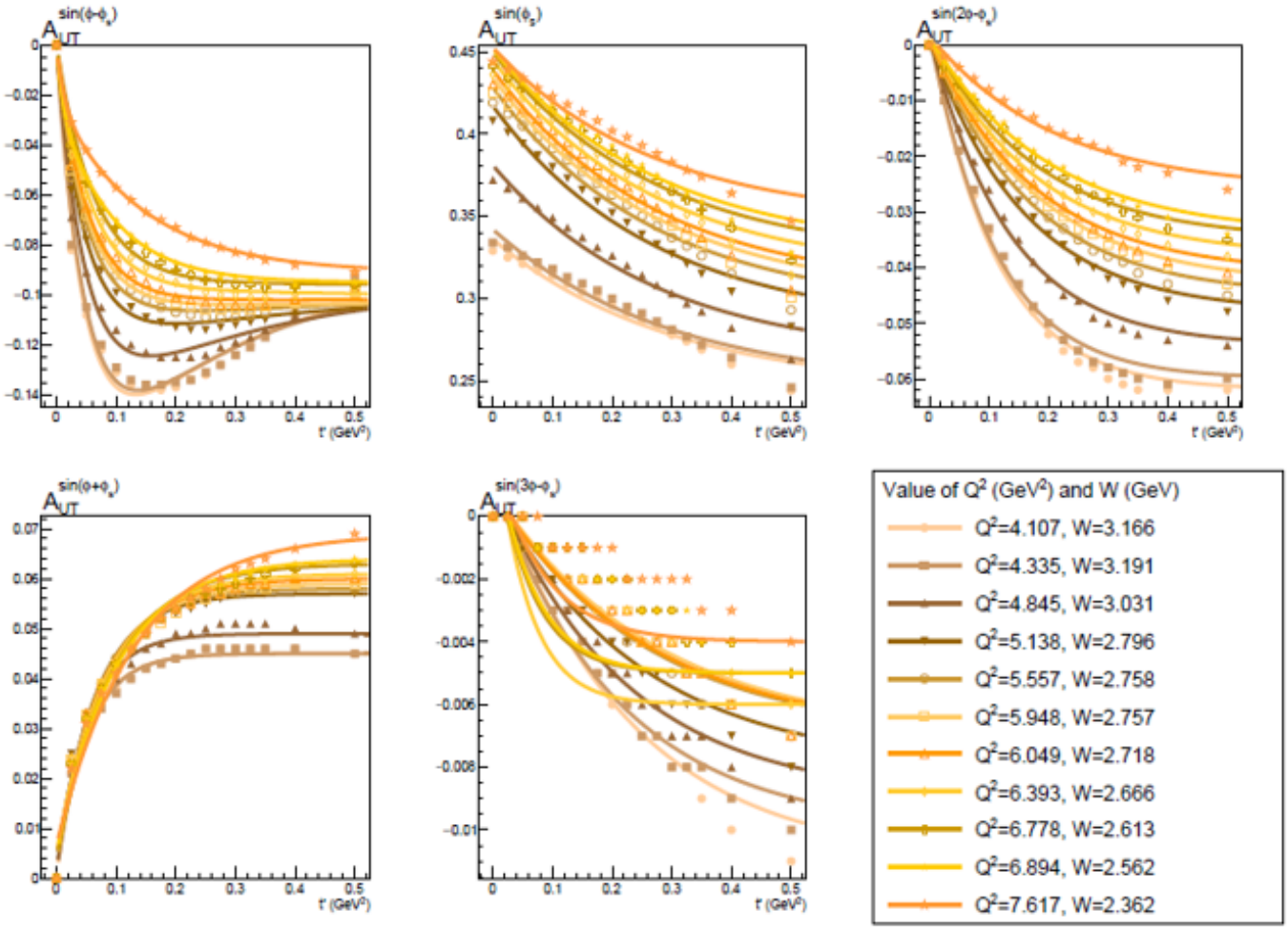

FIG. 9. Asymmetry amplitudes vs t' for different values of Q^2 and W. Data points are the raw model data provided by Goloskokov and Kroll [23]. The lines are the parameterized fit for each Q^2, W pair.

The parameters are saved to a file and read at runtime into instances of the Asymmetry class. Each Asymmetry object corresponds to one of the five asymmetries and contains each of the parameterized functions for that asymmetry, one for each Q^2, W pair. The Asymmetry class implements a function to retrieve the asymmetry amplitude given Q^2 and t' as arguments. The value is calculated by selecting the two functions with the associated values of Q^2 closest to the input. These two functions are each evaluated at the input t' value, resulting in two data points, (Q_1^2, A_1) and (Q_2^2, A_2). A line is then drawn between these two points to interpolate a value for the asymmetry amplitude at the input Q^2 value.

The asymmetries are accessed by the SigmaCalc class and used to calculate the cross section component σ_{UT} according to Equation 33.

$$\Sigma_k = d\sigma_{UU}(\phi) A_{UT}^{\sin(\mu\phi+\lambda\phi_s)_k} \tag{32}$$

$$d\sigma_{UT} = -\frac{P_T}{\sqrt{1-\sin^2\theta\sin^2\phi_s}} \sum_{k=1}^{6} \sin(\mu\phi+\lambda\phi_s)_k \Sigma_k. \tag{33}$$

3. σ and Event Weight

The cross section components σ_{UU} and σ_{UT} are summed to give the overall cross section σ, as shown by Equation 34.

$$d\sigma = d\sigma_{UU} + d\sigma_{UT} \tag{34}$$

Explicitly, this cross section is a two-fold differential scattering cross section in the center of mass frame. In order to calculate the event weight, the five-fold differential cross section in the lab frame is needed. This is calculated as follows

$$d^5\sigma = \frac{d^5\sigma}{dE' d\Omega_{e'} d\Omega_\pi} = \Gamma_V J \frac{d^2\sigma}{dt d\phi} \tag{35}$$

where J is the Jacobian transformation from the center of mass frame to the lab frame. Γ_V is the virtual photon flux factor, defined as

$$\Gamma_V = \frac{\alpha}{2\pi}\frac{E'}{E}\frac{(W^2-M_n^2)}{2M_nQ^2}\frac{1}{1-\epsilon}, \tag{36}$$

where α is the fine structure constant, W is the invariant mass of the final state, and ϵ is the virtual photon polarization, as given by Equation 37.

$$\epsilon = \left(1 + \frac{2|\vec{q}|^2}{Q^2}\tan^2\frac{\theta_e}{2}\right)^{-1}, \tag{37}$$

The event weight is then given by the following expression:

$$w = \frac{d^2\sigma}{d\Omega_\pi}\frac{(\text{phase-space-factor})(\text{luminosity})(\text{target-factors})}{N_{gen}} \tag{38}$$

The phase-space-factor is the fraction of the total kinematically accessible phase space that is covered by the event generator. The luminosity for the SIDIS experiment is 10^{36} $\text{cm}^{-2}\text{s}^{-1}$ [24]. The target-factors include the 60% target polarization and the 85.6% effective polarized neutron of the Jefferson Lab polarized ^{3}He target. N_{gen} is the total number of generated events, including those that were discarded due to either falling outside of acceptable parameters, or having no valid solutions in the kinematics solver.

F. u-channel Exclusive $p(e,e'p\pi^0)$ Physics Model

IV. RESULTS

A. Exclusive $p(e,e'\pi^+)n$ Projections for EIC

We have performed simulations demonstrating the feasibility of pion electric form factor measurements at the EIC using this event generator. DEMP event kinematic distributions are shown in Fig. 10. The neutrons take nearly all of the proton beam momentum and are detected at very forward angles (ZDC). The scattered electrons and pions have similar momenta, except that the electrons are distributed over a wider range of angles, e.g. for 5×100 beam energies, the 5-6 GeV/c electrons are primarily scattered 25-45^o from the electron beam, while the 5-12 GeV/c π^+ are 7-30^o from the proton beam.

The EIC can allow a pion form factor measurement up to Q^2=35 GeV^2, as shown in Fig. 11. The pion form factor projections assume an integrated luminosity of 20 fb^{-1} with a 5 GeV electron beam colliding with a 100 GeV proton beam. We assume:

- Integrated luminosity of 20 fb^{-1} for the 5×100 GeV measurement.
- Clean identification of exclusive $p(e,e'\pi^+n)$ events by tagging the high energy, forward going neutron in the ZDC.
- Systematic uncertainty of 2.5% point-to-point, and 12% scale
- $R = \sigma_L/\sigma_T = 0.013 - 0.14$ at the lowest $-t$, and $\delta R = R$ systematic uncertainty in the model [19] subtraction to isolate σ_L.
- Pion pole channel dominance at small $-t$ confirmed in exclusive π^-/π^+ ratios obtained from $e+d$ collision data.

A consistent and robust EIC pion form factor data set will probe deep into the region where $F_\pi(Q^2)$ exhibits strong sensitivity to both emergent mass generation via DCSB and the evolution of this effect with distance scale.

B. Exclusive $^3\vec{H}e(e,e'\pi^+)p$ Projections for SoLID at Jefferson Lab

The current studies with the event generator are run using the following configuration:

- Beam energy: 11 GeV.
- Scattered electron energy: 1.1 to 9.9 GeV.
- Scattered electron θ: 5° to 27°.
- Pion θ: 6° to 18°.

In addition, any events meeting the following criteria are discarded due to being outside the accurate range for the cross section model:

- $t < -1.2$ GeV^2

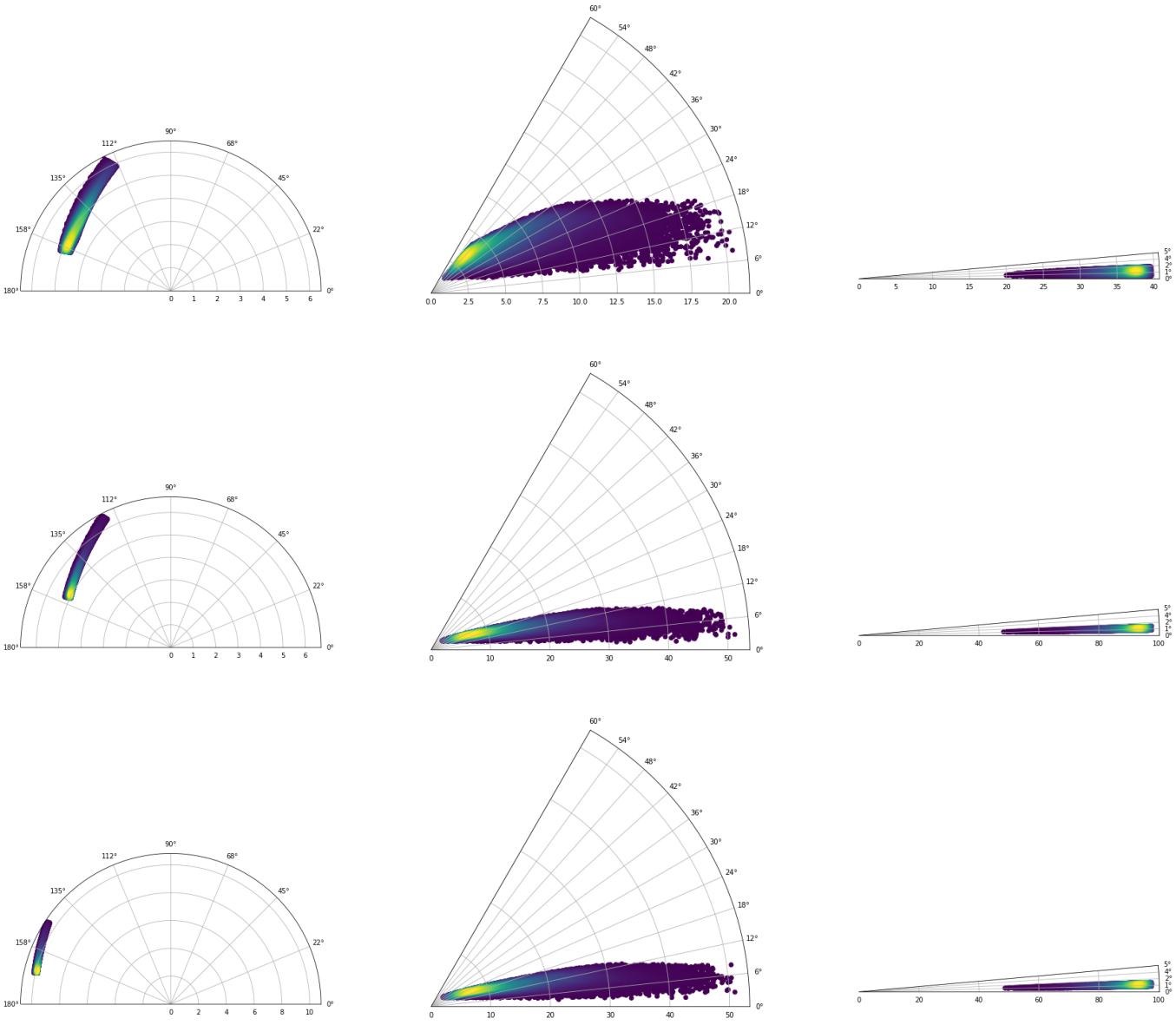

FIG. 10. Exclusive $p(e, e'\pi^+ n)$ kinematic distributions for e' (left), π^+ (center), n (right) at 5×41 (top), 5×100 (middle) and 10×100 (bottom) GeV beam energy combinations. The radial component is momentum, and the polar coordinate is the scattering angle with the proton beam direction to the right and the electron beam direction to the left.

- $Q^2 < 4$ GeV^2
- $W < 2$ GeV

Fig. 12 shows the weighted momentum and polar angle distribution of particles generated in this configuration.

Depending on the quality of data on the recoiled proton provided by SoLID, missing mass and momentum cuts may be necessary in analysis of the data. The missing momentum is also useful in identifying events which have undergone final state interaction (Section IV B 2). The missing mass and momentum are defined in DEMP as follows:

$$\vec{p}_{miss} = \vec{p}_{beam} - \vec{p}_{e'} - \vec{p}_{\pi} \tag{39}$$
$$E_{miss} = E_{beam} + m_n - E_{e'} - E_{\pi} \tag{40}$$
$$m^2_{miss} = E^2_{miss} - p^2_{miss} \tag{41}$$
$$m^2_{miss} = (E_{beam} + m_n - E_{e'} - E_{\pi})^2 - |\vec{p}_{beam} - \vec{p}_{e'} - \vec{p}_{\pi}|^2 \tag{42}$$

1. *Fermi Momentum Effects*

The target neutron in the DEMP experiment is contained within a ^{3}He nucleus. As such, the neutron has a non-zero momentum in the lab frame, known as Fermi momentum. Fermi monentum is incorporated into the event generator in the TargetGen class, which generates the target neutron's

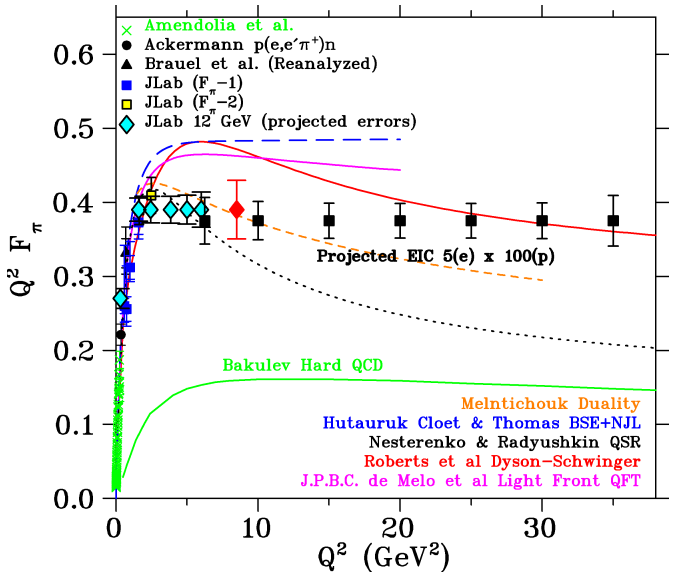

FIG. 11. Existing data (blue, black, yellow, green) and projected uncertainties for future data on the pion form factor from JLab (cyan, red) and EIC (black), in comparison to a variety of hadronic structure models. The EIC projections clearly cover a much larger Q^2 range than the JLab measurements, providing access to the emergent mass scale in QCD.

momentum before the main kinematics calculation is performed. The direction of the neutron's Fermi momentum is chosen uniformly using sphere point picking [12].

The magnitude of the Fermi momentum follows the distribution shown in Fig. 13. This spectral function was produced by a Monte Carlo routine according to the Argonne Nuclear Potential [25].

The data was originally generated with the following normalization:

$$4\pi \int p^2 \frac{dF}{d\vec{p}} dp \sin\theta d\theta d\phi = 2. \tag{43}$$

The distribution was normalized to two in order to describe the two protons in ^{3}He nucleus. For the single neutron, the distribution needs to be normalized to one, as such the data have simply been divided by two and reused in this project.

The resulting momentum distribution is given by a set of 1000 discrete data points, providing the probability density from 0 to 1 GeV/c. As there is no clear, theoretically motivated, functional form for this distribution, the momentum is selected in the generator by a simple Monte Carlo procedure: A point, $(x \in [0, 300], y \in [0, 6.03])$, is randomly selected. If this point lies within the shaded area on Fig. 13, then it is used, otherwise the procedure repeats until a point in the shaded area is found. In order to cut down on computation time, the data is truncated at 300 MeV/c beyond which the probabilities are negligible.

Fig. 14 demonstrates the effect of Fermi momentum on the generated data. The effect of Fermi momentum on the missing mass and momentum distributions is shown in Fig. 15. These plots indicate that the effect of Fermi momentum is minimal.

2. *Final State Interaction Effects*

When the target nucleon emits the charged pion, it is possible for the pion to scatter off of one of the other nucleons in the ^{3}He nucleus as it passes through the nuclear volume. This secondary reaction is known as the Final State Interaction (FSI). A more thorough study on the effects of FSI on DEMP is planned for the future. For the time being however, the effects have been estimated by calculating the kinematics using elastic scattering and the scattering cross section using phase-shift parameterizations by Rowe, Solomon and Landau [26].

FSI is implemented in the event generator using another instance of the TargetGen class to generate a target proton with Fermi Momentum as described in Sec. IV B 1. A random direction is selected with sphere point picking [12] to determine the direction of the scattered pion in the pion-nucleon center of mass frame. In the center of mass frame, the total momentum is zero, so:

$$|p_\pi| = |p_p| = p \tag{44}$$
$$|p'_\pi| = |p'_p| = p' \tag{45}$$

The conservation of energy equation then may be expressed as:

$$E_\pi + E_p = E'_\pi + E'_p \tag{46}$$
$$\sqrt{p^2 + m_\pi^2} + \sqrt{p^2 + m_p^2} = \sqrt{p'^2 + m_\pi^2} + \sqrt{p'^2 + m_p^2} \tag{47}$$

The only solution to this equation is $p = p'$, and so the kinematics of the outgoing particles are trivial.

The implementation of the cross section calculation was written by A. Shinozaki [27], and further modified by us. This code is included in the event generator unmodified in order to calculate the $\pi^- N$ differential scattering cross section.

This differential cross section is given in the center of mass frame, and must be transformed via a Jacobian into a Lab frame value which may be used as a correcting factor to the overall event weight. Three different formulations of the Jacobian are made available.

The "William's Weight" uses the following Jacobian [28]:

$$J_{Williams} = \frac{|p_{\pi,lab}|^2}{\gamma|p_{\pi,com}|(|p_{\pi,lab}| - \beta E_{\pi,lab}\theta_{\pi,lab})} \tag{48}$$
$$\gamma = \frac{E_{\pi,lab} + E_{p,lab}}{|p_{\pi,lab} + p_{p,lab}|} \tag{49}$$
$$\beta = \frac{|p_{\pi,lab}| + |p_{p,lab}|}{E_{\pi,lab} + E_{p,lab}} \tag{50}$$

The "Dedrick Weight" uses the following Jacobian [29]:

$$J_{Dedrick} = \frac{\left((g + \cos^2(\theta_{\pi,com}) + (1-\beta^2)(1 - \cos^2(\theta_{\pi,com}))\right)^{3/2}}{(1-\beta^2)|(1 + g\cos(\theta_{\pi,com}))|} \tag{51}$$
$$g = \frac{\beta E_{\pi,com}}{p_{\pi,com}} \tag{52}$$

where β is the same as in the William's Weight.

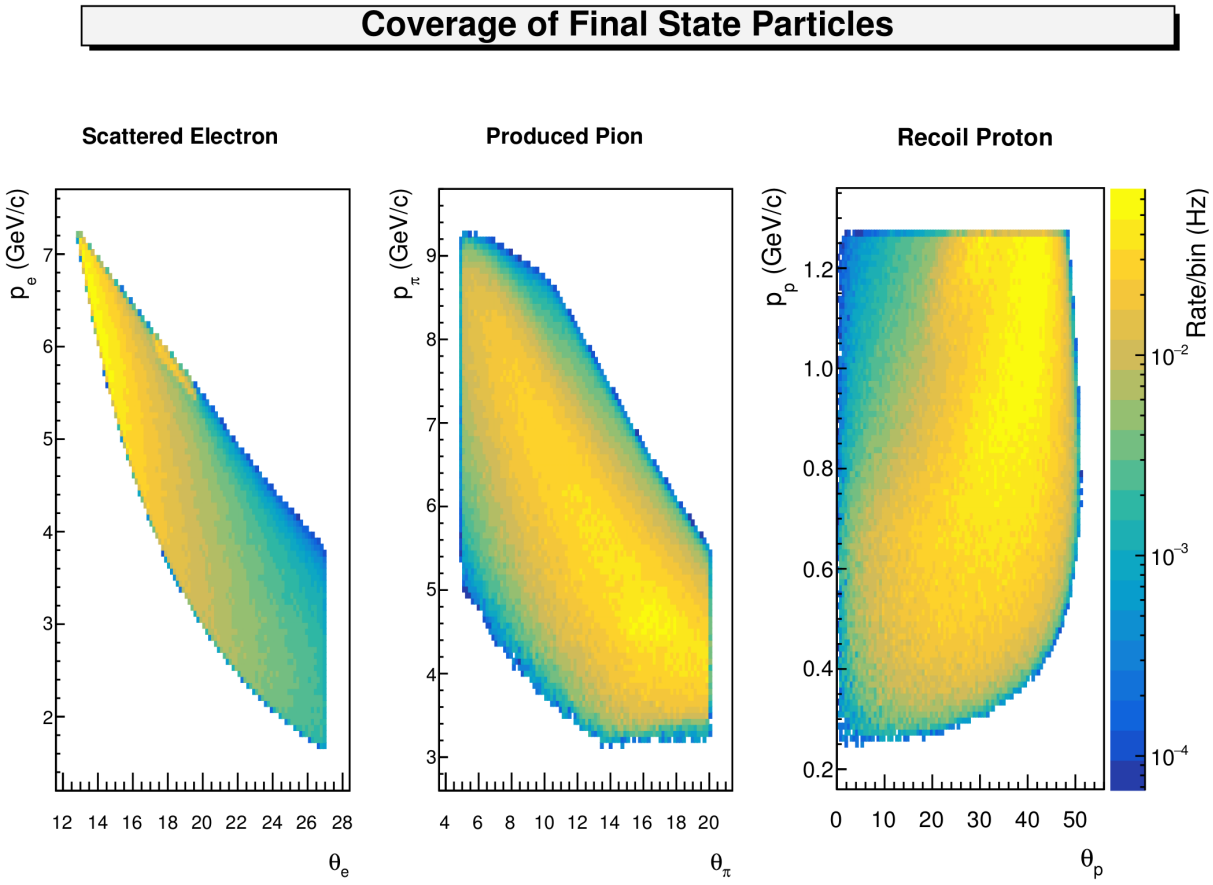

FIG. 12. Weighted kinematic coverage of the three final state particles produced by the DEMP event generator. The color axis represents the rate for each bin.

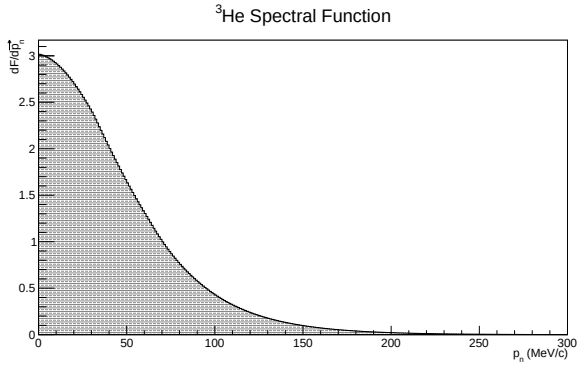

FIG. 13. ^{3}He spectral function generated according to the Argonne Nuclear Potential [25].

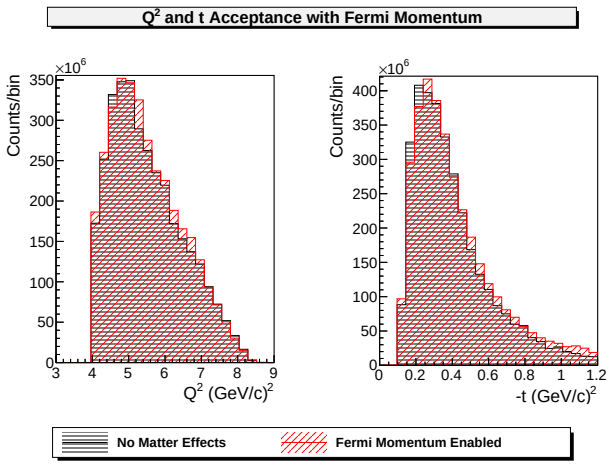

FIG. 14. Comparison of Q^2 (left) and t (right) weighted distribution with Fermi momentum disabled (blue) and enabled (red).

Finally, the "Catchen Weight" uses the following Jacobian [30]:

$$J_{Catchen} = \frac{|p_{\pi,lab}|^2 E_{\pi,com}}{|p_{\pi,com}|^2 E_{\pi,lab}} \tag{53}$$

The effects of FSI on the missing momentum distributions are shown in Fig. 16, using Catchen Weight in weighting the FSI-enabled data. The figure shows that a secondary interaction has a much more significant effect on the data than the other corrective effects. However they also indicate that events which undergo FSI occur at a much smaller rate than those that do not. Furthermore, Fig. 16 indicates that the majority of FSI events can be eliminated by cutting events with $|\vec{p}_{miss}|> 1.2$ GeV/c. Remaining FSI events constitute

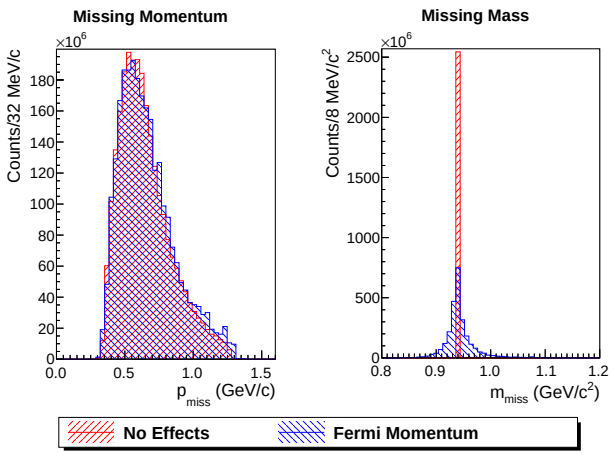

FIG. 15. Missing mass and momentum distribution with only energy loss effects enabled, shown by the red squares. The blue circles indicate data with no corrective effect enabled.

only 4% of events.

C. Exclusive u-channel $p(e, e'\pi^0 p)$ Projections for EIC

V. SUMMARY AND OUTLOOK

[1] Matthias Burkardt, Phys. Rev. D 62 071503(R)
[2] Xiangdong Ji., Phys. Rev. Lett. 78, 610
[3] K.Goeke, M.V.Polyakov and M.Vanderhaeghen., Prog. Part. Nucl. Phys. 47, 401
[4] Frankfurt *et al.*, Phys. Rev. D 60, 014010
[5] A. Accardi *et al.*, arXiv:1212.1701v3 [nucl-ex] 30 Nov 2014
[6] G. M.Huber *et al.*, Phys. Rev. C78, 045203 (2008).
[7] C.E. Carlson, J. Milana, Phys. Rev. Lett., 65, 1717–1720 (1990). https://doi.org/10.1103/PhysRevLett.65.1717
[8] T. Horn, G.M. Huber, P.E. Markowitz, et al., Jefferson Lab Experiment E12-09-011, "Studies of the L–T Separated Kaon Electroproduction Cross Section from 5-11 GeV", http://www.jlab.org/exp_prog/proposals/09/PR12-09-011.pdf
[9] K. Park, et al., Phys. Lett., B780, 340-345 (2018) https://doi.org/10.1016/j.physletb.2018.03.026
[10] W.B. Li, et al., Phys. Rev. Lett., 123, 182501 (2019) https://doi.org/10.1103/PhysRevLett.123.182501
[11] A. Bacchetta, U. D'Alesio, M. Diehl, C.A. Miller. Phys. Rev. D, 70, 117504 (2004) https://doi.org/10.1103/PhysRevD.70.117504
[12] E.W. Wesstein, http://mathworld.wolfram.com/SpherePointPicking.html
[13] R. Brun, E. Rademakers, Nucl. Inst. & Meth. in Phys. Res. A, 289, 81–86 (1996) http://root.cern.ch/
[14] *https://hallcweb.jlab.org/wiki/index.php/SIMC_Monte_Carl*
[15] T.K. Choi, K.J. Kong, B.G. Yu, Byung Geel, J. Korean Phys. Soc., 67, 1089–1094 (2015) https://doi.org/10.3938/jkps.67.1089
[16] S. Basnet, et al. Phys. Rev. C, 100, 065204 (2019) https://doi.org/10.1103/PhysRevC.100.065204
[17] *http://lichen.phys.uregina.ca/index_files/talks/atpi_solid_pac*17.p
[18] Christian Weiss, JLab Theory Report, 30 Jan 2008.
[19] T. Vrancx, J. Ryckebusch, Phys. Rev. C, 89, 025203 (2014) https://link.aps.org/doi/10.1103/PhysRevC.89.025203
[20] T. Vrancx, J. Ryckebusch, Jannes, Phys. Rev. C, 89, 065202 (2014) https://doi.org/10.1103/PhysRevC.89.065202
[21] J. Nys, J. Ryckebusch, http://rprmodel.ugent.be/calc/
[22] H.P. Blok, et al., Phys. Rev. C, 78, 045202 (2008) https://doi.org/10.1103/PhysRevC.78.045202
[23] S. V. Goloskokov, P. Kroll, Private Communications, 2009-2017
[24] The SoLID Collaboration, https://hallaweb.jlab.org/12GeV/SoLID/files/solid_precdr.pdf
[25] R. Schiavilla, V.R. Pandharipande, R.B. Wiringa, Nucl. Phys. A, 449, 219–242 (1986) https://doi.org/10.1016/0375-9474(86)90003-5
[26] G. Rowe, M. Salomon, R.H. Landau, Rubin, Phys. Rev. C, 18, 584–589 (1978) https://doi.org/10.1103/PhysRevC.18.584
[27] A. Shinozaki, Ph.D. Thesis, University of Regina, 2002.
[28] W. S. C. Williams, "An introduction to elementary particles", Appendix B, Academic Press, 1971.
[29] K.G. Dedrick, Rev. Mod. Phys. 34, 429–442 (1962) https://doi.org/10.1103/RevModPhys.34.429
[30] G.L. Catchen, J. Husain, R.N. Zare, J. Chem. Phys., 69, 1737-1741 (1978) https://doi.org/10.1063/1.436749

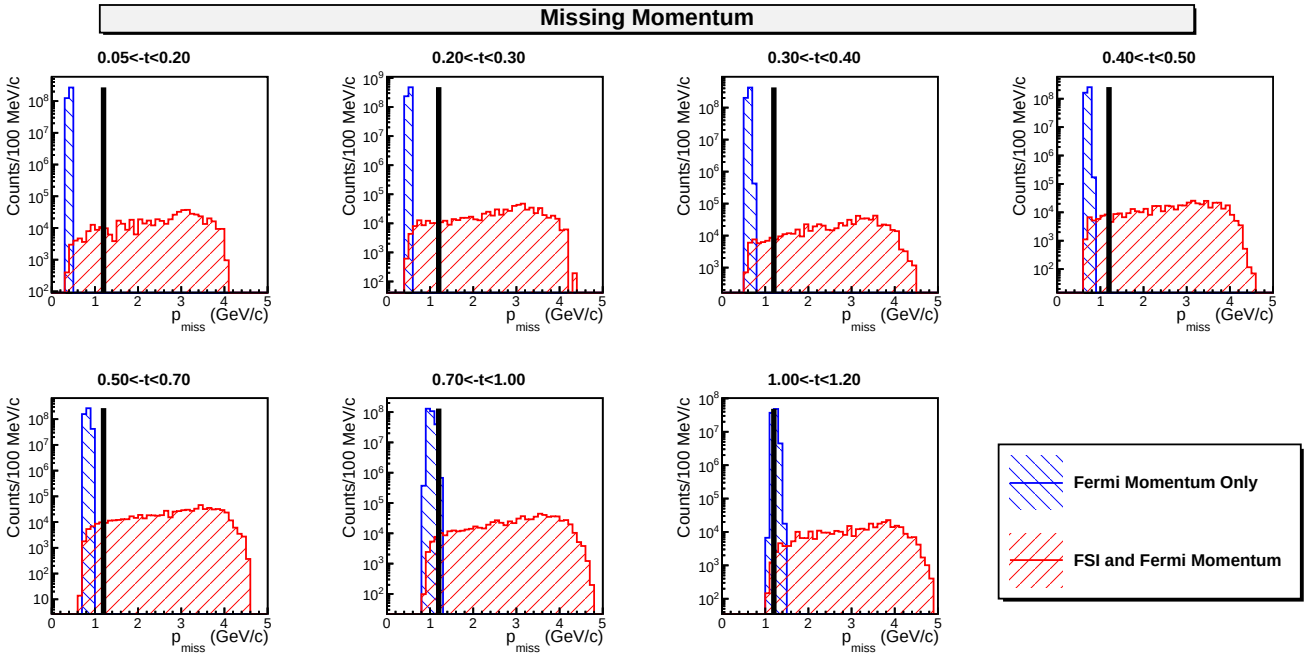

FIG. 16. Weighted missing momentum distribution in each t bin, with FSI and Fermi momentum enabled, compared to the distribution with only Fermi momentum enabled, and with no effects enabled. The FSI distribution uses the Catchen weight in its weighting.